# High-field magnetic birefringence study of the phase behavior of concentrated solutions of phospholipid tubules

S. Sprunt, G. Nounesis, and J. D. Litster
*Francis Bitter National Magnet Laboratory, Massachusetts Institute of Technology, Cambridge, Massachusetts 02139-4307*

B. Ratna* and R. Shashidhar
*Biomolecular Science and Engineering, Code 6900, Naval Research Laboratory, Washington, D.C. 20375*
(Received 26 October 1992)

High-resolution, high-field magnetic birefringence has been used to study the behavior of single-bilayer phospholipid tubules in concentrated solutions and in the vicinity of the lipid chain-melting temperature $T_m$. Results are presented for five different initial lipid densities, $\rho=0.5$, 1.0, 2.0, 4.0, and 6.0 mg/cm$^3$—which yield tubule concentrations in the range $\nu=10^9$–$10^{10}$ cm$^{-3}$—at fields to 15 T. On approach to $T_m$ from room temperature, the maximum induced refractive-index anisotropy $\Delta n_{\max}$ evolves with concentration from a smoothly decreasing to a sharply discontinous function; a sample with concentration corresponding to $\rho=4.0$ mg/cm$^3$ shows evidence of a nearly critical phase transition. Above $T_m$ the system appears isotropic (there is no induced anisotropy), although measurements of the optical transmission $I_T$ indicate that at $T\sim T_m$ and for $\rho\approx 4.0$ mg/cm$^3$, the structure of the isotropic phase changes significantly. For $T$ sufficiently above $T_m$, however, the isotropic phase has the same properties for all $\rho$. The significance of these results is discussed qualitatively in terms of models proposed for tubule formation and phase behavior. Data are also presented for cooling samples in a high field from $T > T_m$. Finally, preliminary measurements indicate that the magnetic susceptibility anisotropy $\Delta\chi$ in the lower concentration samples has a different temperature dependence than the induced refractive-index anisotropy for $T < T_m$.

PACS number(s): 61.30.Eb, 61.30.Gd, 87.15.Da

## I. INTRODUCTION

Among the more fascinating structures formed in lipid solutions is the tubule [1,2], a rigid, hollow cylinder that has walls consisting of one or more bilayers and that may be a few tens to several hundred micrometers in length $L$ and a few tenths to one micrometer in diameter $b$. The biologically important double-chain phospholipids—in particular, the chiral compound 1,2-bis (10,12-tricosadiynoyl)-sn-glycero-3-phosphocholine (abbreviated $DC_{8,9}PC$)—have so far received the most attention in studies of tubule morphology [3]. Tubules composed of these materials are produced in two ways: first [1], for purely aqueous dispersions, by the transformation of large lipid liposomes (diameter $\sim 1$ $\mu$m) cooled below the lipid chain-melting temperature $T_m$, and second [4], for solutions of monomer in a miscible solvent (alcohol), by precipitation when a small fraction of immiscible solvent (water) is added at $T < T_m$. In the latter approach, precise control over tubule dimensions, with minimal polydispersity, is possible by variation of the lipid concentration and solvent composition (e.g., alcohol chain length, water-to-alcohol ratio) [5]. The value of $T_m$ is also dependent on these parameters.

The physical mechanism behind tubule formation is an outstanding problem. Evidence from microscopy suggests that, in the pure-water system, the membranes of liposomes flatten and elongate as the lipid chains crystallize at $T=T_m$, and that the aggregation of several of these distorted structures may provide the nucleus [6] for a tubule. To produce a cylinder, the lipid packing in the crystallized membrane presumably must favor a finite curvature in one direction and zero in the other; to account for this, a collective tilting of the molecules within the bilayer has been suggested [7,8]. For the water-alcohol system (which is generally alcohol-rich), the situation is less clear. Here helical bilayer structures—with regular gaps in the winding—appear to be the tubule precursors [4]; their aggregation, and the closing of the gaps, may lead to complete tubules. Indeed, partially formed tubules have been observed with frayed ends of thin, twisted bilayer strips [9]. Theoretically, Helfrich and Prost have predicted [8,10] that a bilayer strip could curl into the shape of a regular helix as a result of the spontaneous twist of chiral molecules at the edges. The model also incorporates an anisotropic in-layer elasticity, which may arise either from molecular tilt (in which case the bilayer could, in principle, be positionally disordered) or from an anisotropic crystalline phase. An electrostatic mechanism for the buckling of a bilayer ribbon, which also invokes molecular tilt, has been proposed [7]. Finally, Lubensky and Prost [11] have recently shown that tubules can be formed from spherical liposomes (vesicles). In fact, the transformation requires only the development of orientational order (tilt, hexatic, or both) within the bilayer; however, the Frank elastic moduli must have comparable magnitudes to those of a crystalline phase. Experimentally, x-ray diffraction studies [12,13] do indicate

 

the presence of molecular tilt.

Since tubules are rigid objects with typically large aspect ratios ($L/b \sim 100$), in a stable, nonaggregated solution they may be thought of as a classical hard-rod system. This picture has been developed in the work of Rosenblatt and others [14,15] on $DC_{8,9}PC$ tubules, where they studied tubule orientation by external electric and magnetic fields. Because of their large size, the cumulative effect of even a weak molecular susceptibility anisotropy is sufficient to allow tubule alignment in magnetic fields of a few tesla (T). A substantial magnetic birefringence, $\Delta n \sim 10^{-6}$, is produced [14] in semidilute solutions, where the tubule concentration $\nu \sim 10^8 - 10^9$ $cm^{-3}$. Further, for highly concentrated solutions, the transition from a microscopic isotropic to nematic state may be investigated (for instance, in the framework of the Onsager theory for hard rods [16]). Indeed, Rosenblatt and co-workers [17] have observed nematic microstructure for multiple-bilayer tubules grown in an ethanol-water mixture at a concentration well above the nematic limit in the Onsager model; moreover, they have produced a very long-lived bulk nematic phase by subjecting these samples to a large magnetic field for $\sim 10$ h.

The main issue we address in this paper, however, is the transformation of a system of aligned single-bilayer $DC_{8,9}PC$ tubules into an optically isotropic phase, probed through the behavior of the maximum induced magnetic birefringence $\Delta n_{max}$, as a function of temperature and of tubule concentration. For $T \ll T_m$, where the tubules are fully developed, $\Delta n_{max}$ corresponds to saturated orientational order. By "transformation," we include both structural changes in the tubules (a single-particle property) and a (possibly concomitant) change in the magnitude of the orientational order of the system (a collective property). For $T \geq T_m$, the tubules are reported to convert into spherical liposomes in the pure-water system [4,13]; the situation is less clear for the alcohol-rich system, although liposomes are known to form when water is added to a solution of lipid in alcohol at a temperature above $T_m$. Pretransitional effects have not been quantitatively studied in either system.

Our results show that $\Delta n_{max}$, together with an associated measurement of the sample transmission $I_T$, is a very sensitive probe of the transformation of the tubule system, revealing a surprisingly large range of pretransitional effects for $T \rightarrow T_m$ and a quite clear qualitative change in these as a function of tubule concentration. Moreover, our measurements provide evidence that a region of interesting critical behavior exists between the aligned tubule and isotropic phases for a system with original lipid density in the vicinity $\rho = 4.0$ mg/cm$^3$.

## II. EXPERIMENT

The $DC_{8,9}PC$ tubules used in our experiments were prepared at NRL in an 85% methanol–15% water solution (weight percentages), using a version [13] of the precipitation technique, in which water is added to a monomer solution above $T_m$, and the temperature subsequently lowered. The resulting tubules show essentially no residue of loose helices, and are of very uniform dimensions, with mean length $L = 60$ $\mu$m, outer diameter $b = 0.4$ $\mu$m, and well thickness of one bilayer ($\approx 6$ nm).

The concentrations investigated are rather high, with the highest comparable to the theoretical nematic limit [16,18]. The issues of excluded-volume tubule-tubule interactions and tubule aggregation thus arise. In studying the behavior of $\Delta n$ below, we shall consider the former. With regard to the latter, we remark that in our experiments the level of $\Delta n_{max}$, after appropriate equilibration, was essentially reproducible for a given concentration and at the initial (low) temperature. Moreover, $\Delta n_{max}$ scaled approximately linearly with concentration at this temperature, and the shape of $\Delta n_{max}$ versus $T$ was consistent for different samples at fixed concentration and heating rate. Thus, at the maximum field, there was no evidence of significant sample inhomogeneity over the region probed optically ($\approx 400$ $\mu$m in diameter). However, during tubule orientation after removal of a high field, we have observed [19] dynamical effects that may reflect the development of inhomogeneity in isotropic samples. Finally, others have noted [4,13] that $DC_{8,9}PC$ tubules in both aqueous and alcohol-rich solutions do not aggregate to any significant degree, even at relatively high lipid concentrations (several mg/ml).

We report results for solutions with an initial lipid mass density $\rho = 0.5$, 1.0, 2.0, 4.0, and 6.0 mg/cm$^3$. Estimates for the resulting tubule concentration $\nu$ depend on the density of lipid packing in the tubule wall; values for the latter obtained from two different sources [13,17] yield a range $\nu \approx 10^9 - 10^{10}$ studied in our experiments. In fact, we are rather limited in the selection of the lipid concentration by the phase diagram for single-bilayer tubules: for the solvent ratio used, tubules are unstable structures for $\rho < 0.5$ mg/cm$^3$ and lipid sedimentation is observed for $\rho > 6$ mg/cm$^3$. Samples were loaded into sealable cells (316 stainless steel with fused silica windows, 3.2 mm optical path length) at $\sim 18$ °C just prior to the start of an experimental run. In the following, we shall distinguish the samples by the lipid mass densities used to prepare them rather than specific values of the tubule concentration; the former was determined with high accuracy, while the latter is a derived quantity.

Sample cells were contained in a specially designed insert for a 33-mm vertical-bore Bitter magnet at the Francis Bitter National Magnet Laboratory. The insert centers the sample in the magnet bore, allows two-stage temperature control (short-term stability $\approx 0.005$ °C), and provides optical access via an adjustable outer mirror positioned in the path of a laser beam (about 25 cm above the magnet) and two fixed internal mirrors mounted on opposite sides of the sample cell. The mirrors have protected aluminum surfaces that are oriented approximately 45° to vertical. Because the insert does not require radial access to the center of the bore, more standard and higher-field magnets may be used; further, temperature gradients across the cell surface are more effectively reduced. Temperature control is accomplished with an

internal resistive heater (Manganin wire, wrapped to minimize the Lorentz force induced by changing field), which is powered by a feedback servo circuit, and an outer jacket connected to a recirculating water bath.

High-resolution magnetic-birefringence measurements are carried out in the usual way [20], which utilizes equal components of sinusoidally phase-modulated laser light polarized along the field (**H**) and unmodulated light polarized perpendicular to **H**, photodetection of the depolarized contribution from this combination which is transmitted through the sample, and recovery of the sample-induced dc phase shift between the original polarizations via a lock-in amplifier referenced to the modulator drive signal. For modulation frequency $\omega_M$ and amplitude $A$, the intensity at the photodetector may be written [21]

$$I(t)=I_{\rm dc}(A)+\sum_{n=1}^{\infty}[I_{2n-1}(A)\sin(2n-1)\omega_M t + I_{2n}(A)\cos 2n\omega_M t] . \quad (1)$$

Our apparatus uses a photoelastic modulator, which has $\omega_M=50$ kHz and $A$ set to 0.75 rad, and a photodiode detector. Experimentally, we shall only be interested in explicit forms for the lowest-order coefficients, which may be calculated as [21]

$$\begin{aligned} I_{\rm dc}&=I_0[1+D^2-2DJ_0(A)\cos\phi] , \\ I_1&=-4I_0DJ_1(A)\sin\phi , \\ I_2&=-4I_0DJ_2(A)\cos\phi , \end{aligned} \quad (2)$$

where $I_0$ is the average *transmitted* intensity, $J_n$ are ordinary Bessel functions of order $n$, and $\phi=\phi_s+\phi_0$, with $\phi_s$ the dc phase shift induced in the sample by the field and $\phi_0$ a phase shift produced by a Soleil-Babinet compensator. The parameter $D$ reflects the preferential absorption (or scattering) of light polarized along **H** relative to that polarized perpendicular to **H**; $D=1$ for isotropic transmission.

The output voltages of two lock-in amplifiers, referenced to $\omega_M$ and $2\omega_M$, give

$$V(\omega_M)=C_1I_1 , \quad V(2\omega_M)=C_2I_2 , \quad (3)$$

where $C_1, C_2$ are fixed parameters characteristic of the lock-in and detector. In addition, we record the dc offset

$$V_{\rm dc}=C_{\rm dc}I_{\rm dc} . \quad (4)$$

Using $\Delta n\equiv n(\|\mathbf{H})-n(\perp\mathbf{H})=kl\phi_s$, where $k=2\pi/\lambda$ for $\lambda=633$ nm and $l=3.2$ mm is the path length through the sample, we obtain from (1)–(3)

$$\Delta n=\frac{1}{kl}\tan^{-1}\left[C_0\frac{V(\omega_M)}{V(2\omega_M)}\right]-\frac{\phi_0}{kl} \approx \frac{C_0}{kl}\frac{V(\omega_M)}{V(2\omega_M)}-\frac{\phi_0}{kl} , \quad (5)$$

where $C_0\equiv C_2/C_1$ and the last equation applies only for small $\Delta n$ (i.e., $\Delta\phi\ll\pi/2$). For small fields and negligible interparticle interactions, one may show from Eqs. (8) and (9) below that $\Delta n\approx C_{\rm CM}H^2$, which defines the Cotton-Mouton constant $C_{\rm CM}$ for the sample under study (and at a fixed $\lambda=633$ nm). In practice, we obtained $C_0$ by calibrating our apparatus with toluene (loaded into an identical sample cell), which has [22] $C_{\rm CM}=3.27\times10^{-9}$ $\rm T^{-2}$. The lock-in output voltages then yield $\Delta n$ according to (5). For an empty cell, $\Delta n$ is stable to $\sim5\times10^{-9}$ over the typical data collection time. (The chief limitations here are the short sample path length $l$ and vibrations associated with the very long optical path necessary to keep a ferromagnetic optical table a safe distance from the magnet. However, the very slow orientational fluctuations of the tubules produced a much larger instability in $\Delta n$ in zero field.) A measure of the transmitted intensity $I_T$ was obtained from $V(2\omega_M)/\cos\phi$ (when $\phi\sim0$) or $V(\omega_M)/\sin\phi$ (when $\phi\sim\pi/2$).

Measurements of the temperature, $V(\omega_M)$, $V(2\omega_M)$, $V_{\rm dc}$, and the field level were made at typically 4-sec intervals on a scanning digital voltmeter, and recorded for computer analysis. In a typical experimental shift, the field was swept up at low temperature (tubule phase), $\Delta n$ was observed to equilibrate, and the temperature was changed at constant field in a series of steps, with $\Delta n$ allowed to stabilize at each step.

## III. EXPERIMENTAL RESULTS AND DISCUSSION

We first review the theory for the induced optical anisotropy for a solution of $\nu$ diamagnetic particles (tubules) per $\rm cm^3$ in a magnetic field $\mathbf{H}\|\mathbf{z}$. We consider the fully developed tubules as hard rods. The refractive-index anisotropy may be written [23,24]

$$\Delta n=n_{\|}-n_{\perp}=\frac{1}{2n_0}\left[\frac{n_0^2+2n_S^2}{3n_S^2}\right]^2\nu\Delta\alpha \times\langle\cos^2\theta-\sin^2\theta\cos^2\phi\rangle . \quad (6)$$

In this expression, $\theta,\phi$ are polar and azimuthal angles specifying the orientation of the tubule long axis, $\mathbf{u}=(\sin\theta\cos\phi, \sin\theta\sin\phi, \cos\theta)$, relative to **H**. (We also choose the $y$ axis along the direction of the incident light, **k**.) $n_0$ is the refractive index of the isotropic solution, and $n_S$ that of the solvent. (The validity for tubules of the coefficient [23] used in (6) is discussed in the Appendix.) The average $\langle\ \rangle$ is taken over **u** (or equivalently, $\theta,\phi$) and is weighted by the Boltzmann factor for the orientational energy of the tubules, $U(\mathbf{u})=U_{\rm MF}(\mathbf{u})+U_{\rm ext}(u_z)$. Here $U_{\rm MF}$ is a mean-field potential accounting for an excluded-volume interaction in concentrated solutions of hard rods, $\nu\sim(bL^2)^{-1}$, and favoring local alignment of the rods. If $\Psi(\mathbf{u})$ describes the probability a rod has orientation **u**, we have [16,18]

$$U_{\rm MF}(\mathbf{u})=2\nu bL^2\int d\mathbf{u}|\mathbf{u}\times\mathbf{u}'|\Psi(\mathbf{u}') . \quad (7)$$

$U_{\rm ext}$ is the potential energy due to the applied field,

$$U_{\rm ext}(u_z)=-\tfrac{1}{2}\Delta\chi H^2u_z^2 . \quad (8)$$

$\Delta\chi$ is the diamagnetic susceptibility anisotropy *per tubule*

(for an orientation of the long axis along versus one perpendicular to **H**), which is essentially a sum over orientations of the constituent $DC_{8,9}PC$ molecules. Finally, $\Delta\alpha$ in (6) is the tubule optical polarizability anisotropy, which includes a molecular contribution $\Delta\alpha^M$ and a geometrical or "form" contribution $\Delta\alpha^F$, due to the tubule shape. (For estimates of these, see the Appendix.)

Defining $\Delta n_{\max}$ as the maximum obtainable $\Delta n$ for completely aligned tubules, given by the coefficient on the right-hand side of (6), and using (7) and (8), we have

$$\Delta n(H,U)=\Delta n_{\max}\frac{\int d\mathbf{u}(u_z^2-u_x^2)\exp\left[\frac{\Delta\chi H^2}{2k_BT}u_z^2-U\int d\mathbf{u}|\mathbf{u}\times\mathbf{u}'|\Psi(\mathbf{u}';\mathbf{H})\right]}{\int d\mathbf{u}\exp\left[\frac{\Delta\chi H^2}{2k_BT}u_z^2-U\int d\mathbf{u}|\mathbf{u}\times\mathbf{u}'|\Psi(\mathbf{u}';\mathbf{H})\right]}\ . \tag{9}$$

Here $U\equiv 2\nu bL^2$, and we have noted that the distribution function will depend on **H**. For $\nu bL^2\ll 1$ or a noninteracting system ($U=0$), (9) becomes

$$\Delta n(H,0)=\Delta n_{\max}\frac{\int_0^1 du_z(u_z^2-\frac{1}{3})\exp\left[\frac{\Delta\chi H^2}{2k_BT}u_z^2\right]}{\int_0^1 du_z\exp\left[\frac{\Delta\chi H^2}{2k_BT}u_z^2\right]}\ , \tag{10}$$

which is an explicit function of $H$. We stress that the form we have used for the interactions assumes $L\gg b$; for $L\to b$, we obtain strictly a *noninteracting* model.

For $\nu bL^2\sim 1$ but $\nu$ below the threshold for true nematic order, the Onsager theory predicts a phase separation into isotropic and nematiclike domains at zero field. We have, in fact, observed evidence of aligned domains at $H=0$ for very large $\nu$. The inset in Fig. 1 shows data for $\Delta n(0,U)$ as a function of temperature for $T\to T_m$ and at $H=0$ in a sample with $\rho=1.0$ mg/cm$^3$; clearly, there is a substantial offset for $T\ll T_m$, which decreases continuously on approach to $T_m$. The state at $T>T_m$ was determined to be isotropic by applying a high field and observing no change in $\Delta n$. In our lower-concentration samples, we have found that a zero-field system with a nearly isotropic distribution in **u** at $T<T_m$ may be achieved if we start with a well-mixed sample and cycle $H$ from zero to a few tesla several times, letting the sample birefringence equilibrate after each change in $H$. However, we have not investigated the long-term stability of the isotropic distribution so obtained.

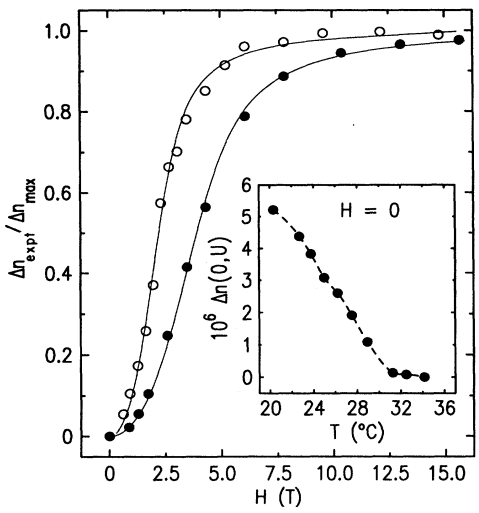


FIG. 1. Magnetic-field dependence of the induced refractive-index anisotropy for $\rho=1.0$ mg/cm$^3$; $\Delta n_{\rm expt}$ is defined in (11). The solid lines are fits to (10) used to obtain values for $\Delta\chi$. The temperature $T=20.38$ °C for the open circles,and 30.83 °C for the closed circles. The inset shows a typical *zero-field* scan of $\Delta n$ versus $T$, revealing in particular the presence of anisotropic domains at low $T$. $\Delta n$ at $T=20.32$ °C is about 25% of the saturated value.

We now consider our results for the field dependence of $\Delta n$. The measured $\Delta n$ is

$$\Delta n_{\rm expt}=\Delta n(H,U)-\Delta n(0,U)\ , \tag{11}$$

with the right-hand side given by (9), and $\Delta n(0,U)\approx 0$ if the initial distribution is approximately isotropic. In Fig. 1, we plot data for $\Delta n_{\rm expt}(H)/\Delta n_{\max}$ versus $H$ at temperatures well below and close to $T_m\approx 33$ °C for $\rho=1.0$ mg/cm$^3$; the solid lines are fits of the data to the *noninteracting* model (10). In the latter, two parameters, $\Delta n_{\max}$ and $\Delta\chi/2k_BT$, are varied. The maximum induced anisotropies are $\Delta n_{\max}=1.8\times 10^{-5}$ for $T=20.38$ °C and $\Delta n_{\max}=1.7\times 10^{-6}$ for $T=30.83$ °C. The data were taken by sweeping the field to fixed levels, and allowing $\Delta n_{\rm expt}$ to settle at each level. Figure 2 shows the scaling of $\Delta n_{\rm expt}$ at temperatures close to $T_m$. In all cases, the initial ($H=0$) states were nearly isotropic: At $T=30.83$ °C, the inset to Fig. 1 shows $\Delta n(0,U)\approx 0\ll\Delta n_{\max}$. On the other hand, at $T=20.38$ °C, where, from the inset, $\Delta n(0,U)$ may be considerable, we obtained an isotropic initial state by the method mentioned above; the value of $\Delta n_{\max}$ is thus essentially identical to that determined by heating the tubules above $T_m$ in high field (see Fig. 3 below).

From Fig. 1, we observe that $\Delta n_{\rm expt}$ at $T=20.38$ °C saturates in a field substantially lower than at $T$ close to $T_m$, where, from Fig. 2, the saturating field is constant. Because of the long equilibration times and the difficulty of obtaining consistent data at low fields, we do not yet have sufficient low-temperature data to determine precisely the crossover in the saturating field. Indeed, for $T_m-T\leq 4$–5 °C, the data for $\Delta n_{\rm expt}(H)$ scale very well to

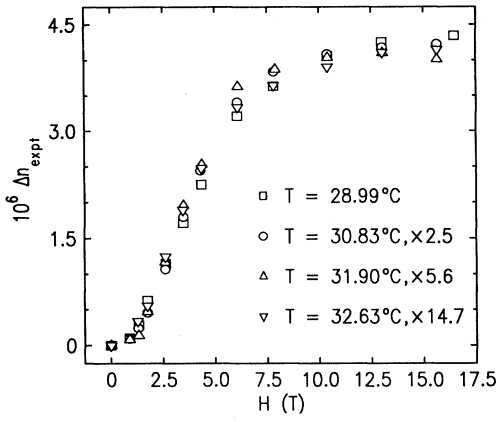


FIG. 2. Scaling of the field dependence of $\Delta n$ near $T_m$ for $\rho=1.0$ mg/cm$^3$. The values of $\Delta\chi$ are evidently very similar for the temperatures studied.

each other. Although we see from the magnitude of the scaling that $\Delta n_{\max} \propto \Delta\alpha$ is a very strong function of temperature for $T\rightarrow T_m$, this similarity in the shape of $\Delta n_{\text{expt}}(H)$ implies that the magnitude of the coupling to the field $\Delta\chi$, which may depend both explicitly and implicitly (through particle-particle interactions) on $H$, is relatively insensitive to $T$ close to $T_m$. (We could not study a region $T_m - T \leq 0.5\,°\text{C}$, where $\Delta n_{\max}\rightarrow 0$ and the data were quite noisy.) Finally, while we expect a significant hard-rod interaction at low temperatures, and do observe in Fig. 1 that the fit is of poorer quality in the region where $\Delta n_{\text{expt}}$ is more rapidly changing ($H\sim 1$–$5$ T), the data evidently have the qualitative behavior predicted by the noninteracting model (10). For $T=20.38\,°\text{C}$, the fit gives an effective $\Delta\chi=5.7\times10^{-14}$ erg/T$^2$; at $T=30.83\,°\text{C}$, we obtain $\Delta\chi=1.9\times10^{-14}$ erg/T$^2$.

To understand the qualitative agreement with (10), we first note that, for $T\rightarrow T_m$, (10) is consistent with a pretransitional behavior that involves a reduction in the length $L$ of the hard-rod core (i.e., a reduction in the excluded-volume interaction). At a lower temperature, however, where the system is very anisotropic, we must look more closely at the full result (9). If the initial distribution is nearly isotropic, $\Psi\rightarrow 1/4\pi$, (7) implies $U_{\text{MF}}\rightarrow \pi\nu bL^2/2$, and (9) reduces to (10) for low fields, which yields $\Delta n_{\text{expt}} \propto \Delta n_{\max}\Delta\chi H^2$. On the other hand, at high fields, $\Delta\chi H^2$ is large and $|\mathbf{u}\times\mathbf{u}'|\approx 0$, so $U_{\text{MF}}$ is negligible compared to $U_{\text{ext}}$, and again (10) should be a good approximation. To assess the relative contributions of $U_{\text{MF}}$ and $U_{ext}$ at intermediate fields, we consider the orientational order parameter $S=\langle 3\cos^2\theta/2-\frac{1}{2}\rangle$. Taking $S=\frac{1}{2}$ at $H=2.5$ T, $\langle\cos^2\theta\rangle=\frac{2}{3}$, so $|U_{\text{ext}}|\sim\Delta\chi H^2\langle\cos^2\theta\rangle/2\approx\Delta\chi H^2/3=8.8k_BT$ (using the fitted value $\Delta\chi=5.7\times10^{-14}$ erg/T$^2$), whereas $|U_{\text{MF}}|\sim 2\nu bL^2\langle\sin\theta\rangle k_BT\approx 1.8k_BT$. Thus, even at intermediate fields, we may self-consistently assume that $U_{ext}$ plays the more substantial role in the field dependence of (9), so again it is not surprising that (10) gives a fair representation of the data.

At $T=20.38\,°\text{C}$, where the tubules are fully formed, we may use $b=0.4$ $\mu$m and $L=60$ $\mu$m to estimate a susceptibility anisotropy per unit volume of the wound bilayer, $\Delta\chi_m\approx-\Delta\chi/\pi bL\delta=-1.3\times10^{-9}$ erg/cm$^3$/G$^2$. Here $\delta$ is the wall thickness, $\delta=6$ nm, and the minus sign reflects the fact that we now reference the anisotropy to the bilayer normal, which lies perpendicular to the field when the tubule long axis is parallel to **H**. This value is about a factor of 5 less than that reported [14] for $DC_{8,9}PC$ tubules grown in ethanol solution, which have $b=0.75$ $\mu$m and $L=20$ $\mu$m and have wall thicknesses of two or three bilayers. The discrepancy may arise due to the sensitive dependence of $\Delta\chi_m$ on the confirmation of the lipid molecules in the tubule wall resulting from the presence of a molecular tilt [12,13] with respect to the tubule surface normal. This would combine the effects of intrinsic (i.e., smectic-$C$) tilt in the bilayer and the pitch of the helical winding; the effect can be substantial [14]. We might also expect a variation of the intrinsic tilt between single- and multiple-bilayer tubules, and of the pitch between alcohol-and water-rich systems.

The limited data of Figs. 1 and 2 suggest a change in the molecular orientation within the bilayer upon heating, which occurs substantially below the temperature $T_m$ at which the system ultimately becomes optically isotropic ($\Delta n=0$). We shall discuss aspects of the phase transformation at $T_m$ in our presentation of results for $\Delta n_{\max}$. However, we should stress here that the measurements in Figs. 1 and 2, from which we study $\Delta\chi(T)$, were taken after temperature changes in *zero* field, whereas $\Delta n_{\max}(T)$ was necessarily studied at a *high* field. This difference may be important. Nevertheless, since the molecular orientation in the tubule wall should be closely related to the tubule structure, a more complete picture of the temperature dependence of $\Delta\chi$ could provide very interesting information on structural changes for $T\rightarrow T_m$, which would complement a study of $\Delta n_{\max}(T)$.

We now turn to the temperature dependence of $\Delta n_{\max}$. Our temperature scans consist of discrete temperature steps (300 mK at room temperature continuously de-

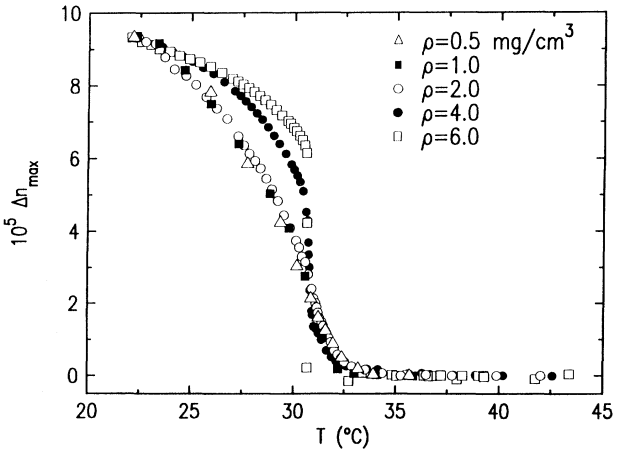


FIG. 3. Maximum induced refractive-index anisotropy $\Delta n_{\max}$ versus $T$ for five different tubule concentrations $\nu$. The field was fixed at 15 T. The data are scaled to match the value at $\rho=6.0$ mg/cm$^3$ and $T=22\,°\text{C}$. The scaling factors are given in the text.

creasing to 50 mK at $T=T_m$), at a constant applied field $H\approx 15$ T (for which $\Delta n\approx\Delta n_{\max}$), with an average waiting period of 10–15 min to allow both the temperature and birefringence to equilibrate.

Figures 3 and 4 display data obtained for heating samples from room temperature through $T_m$ for five different concentrations $\rho=0.5$, 1.0, 2.0, 4.0, and 6.0 mg/cm$^3$. The data presented in Fig. 3 have been scaled to $\Delta n_{\max}$ for the $\rho=6.0$ mg/cm$^3$ sample at $T=22$ °C. The scaling factors are 1.5 for the 4.0, 3.0 for the 2.0, 5.0 for the 1.0, and 13 for the 0.5 mg/cm$^3$ samples, so that except for a somewhat low value at 1.0 mg/cm$^3$, $\Delta n_{\max}$ scales remarkably well with $\rho$ at room temperature. This result strongly suggests that well below $T_m$, where the tubules are fully developed, the aligned system is homogeneous and that aggregation is not significant. Because, as is shown in the Appendix, the major contribution to $\Delta n_{\max}$ comes from shape anisotropy, it also confirms that the tubule size distribution is sharply peaked at a consistent value. A second remarkable feature in Fig. 3 is that the temperature dependence of $\Delta n_{\max}$ scales for the three lowest concentrations at all temperatures. This indicates that for the more dilute solutions, the mechanism and thermodynamics of the phase transformation are identical. For all five concentrations, $\Delta n_{\max}$ decreases monontonically to zero with increasing temperature (indicating an isotropic system at $T>T_m$). As mentioned above, and as is demonstrated in the inset to Fig. 4, the high-temperature isotropic state is characterized by a lack of any response in $\Delta n$ to removal of the field. However, for $\rho\geq 4.0$ mg/cm$^3$, we observe a striking change in the behavior of $\Delta n_{\max}(T)$.

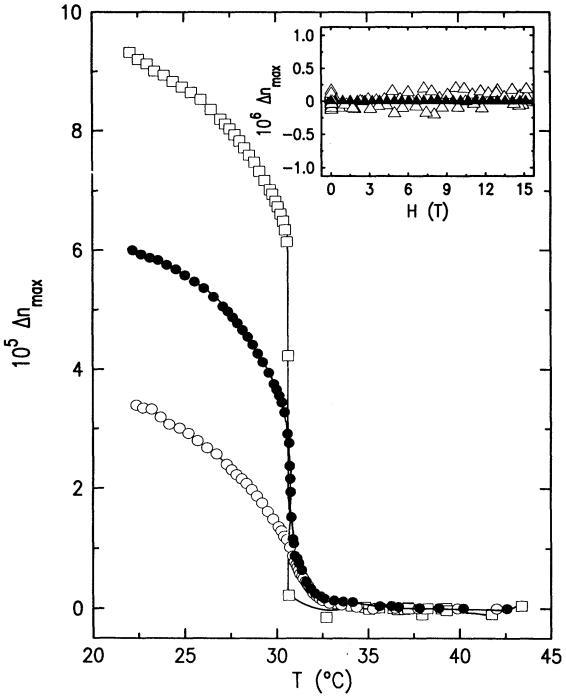


FIG. 4. $\Delta n_{\max}$ vs $T$ for three tubule concentrations $\nu$ and $H=15$ T: $\rho=2.0$ (open circles), $\rho=4.0$ (solid circles), and $\rho=6.0$ mg/cm$^3$ (open squares). The solid lines are guides to the eye. For $\rho=6.0$ mg/cm$^3$, accurate data could not be obtained for $T_m\leq T<33$ °C because of a very small and fluctuating transmitted intensity. The inset shows the effect of a field sweep for $T>T_m$ and $\rho=6.0$ mg/cm$^3$; there is no induced birefringence, indicating an isotropic system. $T=39.25$ °C for the open triangles (isotropic coexistence region), and $T=43.36$ °C for the solid triangles (nearly transparent isotropic phase). Similar results are obtained at $T>T_m$ for $\rho=2.0$ and $\rho=4.0$ mg/cm$^3$.

This change is highlighted in Fig. 4, where we present the unscaled data for $\Delta n_{\max}$ for samples with $\rho=2.0$, 4.0, and 6.0 mg/cm$^3$. While both the $\rho=2.0$ mg/cm$^3$ and $\rho=4.0$ mg/cm$^3$ systems evolve continuously to the isotropic state, it is clear that, near $T_m$, their temperature dependence is quite different. The data for $\rho=2.0$ mg/cm$^3$ are quite rounded near $T_m$, whereas those for $\rho=4.0$ mg/cm$^3$ display a much sharper temperature dependence. The data were obtained at thermodynamic equilibrium—i.e., temperature stability $<2$ mK, and $\Delta n_{\max}$ and the sample transmission equilibrated to about 2%. Therefore, the continuity and rounding observed at lower $\rho$ do not reflect any artifacts that might arise from a too rapid scan of the temperature. The situation for $\rho=6.0$ mg/cm$^3$ is again different. Here $\Delta n_{\max}$ exhibits a *discontinuous* jump to an isotropic phase. Accurate data in the region $T_m\leq T\leq 33$ °C—i.e., just above the transition—could not be obtained due to a combination of a very low level of the transmitted intensity $I_T$ and substantial fluctuations in this level; at somewhat higher $T$, though still for low $I_T$ (see Fig. 5), the latter were alleviated.

The temperature dependence of $I_T$ also shows striking differences among the samples with $\rho=2.0$, 4.0, and 6.0 mg/cm$^3$. The results, obtained at $H=15$ T, are presented in Fig. 5. For $\rho=2.0$ mg/cm$^3$, $I_T(T)$ rises smoothly with $T$; at $T\approx T_m$, it takes a small dip before rising to a level that corresponds to a nearly transparent isotropic phase, which shows no evidence of a tubule morphology. $I_T$ at $\rho=4.0$ mg/cm$^3$ behaves similarly for $T<T_m$, but at $T_m$ it decreases abruptly to a level about 25 times lower than that for $T\ll T_m$, and, following a change of $\sim 0.2$ °C, increases as abruptly to an intermediate level, where it remains constant for $\sim 0.7$ °C before eventually attaining the isotropic level of the $\rho=2.0$ mg/cm$^3$ sample at $T\approx 36$ °C. Evidently, the small dip in $I_T$ for $\rho=2.0$ mg/cm$^3$ evolves into a very substantial transitional turbidity at the higher concentration. The trend continues for $\rho=6.0$ mg/cm$^3$, where the regions of extreme and intermediate turbidity for $T>T_m$ are substantially broader ($\sim 4.5$ °C and 7 °C, respectively). The transparent isotropic phase is fully established at significantly higher $T$, $T\approx 43$ °C.

Comparing only the lowest- and highest-temperature behavior, we see that the tubule concentration affects $I_T$ much more strongly in the (aligned) tubule phase than in the high-$T$ isotropic phase; this clearly indicates a structural change. Moreover, since Fig. 5 demonstrates that, within the limitations of our measurements very close to $T_m$, the turbid phases observed at $\rho=4.0$ and 6.0

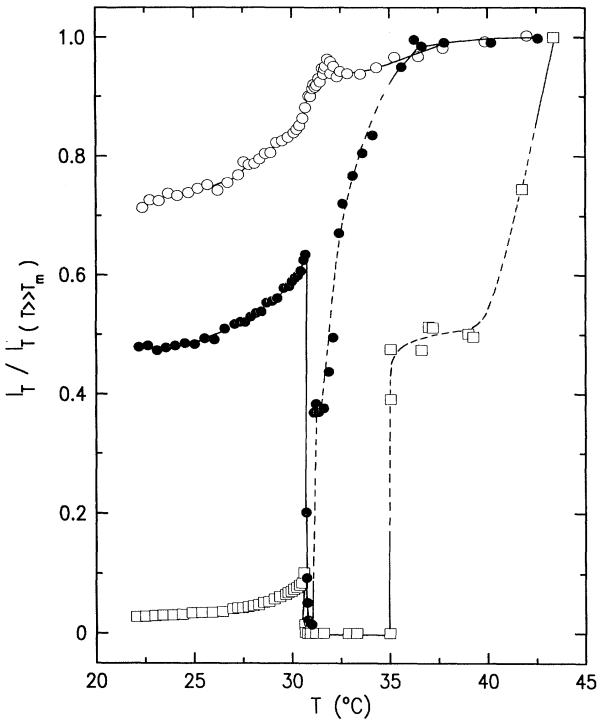


FIG. 5. Transmitted intensity $I_T$ vs $T$ for the same tubule concentrations presented in Fig. 4, using the same symbol code. The data have been normalized to 1 at the isotropic phase level for $\rho=2.0$ mg/cm$^3$. The dashed line for $\rho=6.0$ mg/cm$^3$ indicates a coexistence region between turbid and nearly transparent isotropic phases.

mg/cm$^3$ are also isotropic ($\Delta n_{\max}\approx 0$), we conclude that isotropic phases composed of particles of quite different size occur at the higher concentrations. The regions of intermediate turbidity for these samples might reflect a coexistence between these phases. In fact, we find that both the width of the coexistence, and, to a lesser degree, the temperature at which $I_T$ (and, for $\rho=6.0$ mg/cm$^3$, $\Delta n_{\max}$) jumps discontinouously, depend on the rate of heating. Significant superheating of both the tubule and (at $\rho=6.0$ mg/cm$^3$) the turbid isotropic phases is therefore observed.

To discuss in more detail the nature of the tubule-isotropic transition, we express Eq. (9) as a function of temperature,

$$\Delta n(T,H)=\Delta n_{\max}(T)S(T,H)\ , \tag{12}$$

where we assume only that the orientational distribution is azimuthally symmetric about **H**, and where $S$ is the orientational order parameter. Since the molecular contribution $\Delta n^M_{\max}$ should be small compared to the form birefringence $\Delta n^F_{\max}$ when tubules are present (see Appendix), we expect $\Delta n_{\max}\approx\Delta n^F_{\max}$ in (12) for $T$ not too close to $T_m$. $\Delta n^F_{\max}$ is a function of the particle dimensions ($L,b$ for a tubule) along and perpendicular to **H**, and hence is directly related to the structure. $\Delta n^M_{\max}$ depends on the orientation of the molecular long axis within the tubule wall; for a helically wound bilayer, this will also depend on $L,b$ through the pitch of the winding. A transcendental equation for $S(T,H)=\Delta n/\Delta n_{\max}$ may be obtained from (9) using, on the right-hand side, an approximation [18] for the excluded-volume interaction, which yields an expression identical to the Maier-Saupe model [25] for low-molecular-weight nematics.

From (12), we see that $\Delta n$ may approach zero as $T\rightarrow T_m$ due either to structural changes in the tubule or (perhaps related) effects in the orientational order. The possibility of an effect on $S$ may be investigated using the Maier-Saupe model [26]. The important result is that when $\Delta\chi H^2\gg k_BT$, $S\approx 1$ for *any* value of the strength $U$ of the mean-field interaction; only for $\Delta\chi H^2<k_BT$, does $S\approx 0$ become possible (and is the only solution for sufficiently small $U$). Therefore, orientational disordering contributes significantly to the pretransitional behavior of $\Delta n_{\max}$ *only* if there is a very large decrease in the (low-temperature) value of $\Delta\chi$, a parameter that may also reflect the particle structure. However, at least at the lower concentrations, we found above that $\Delta\chi H^2>10^2k_BT$ for $H=15$ T even quite close to $T_m$. We conclude that $\Delta n_{\max}(T)$ plays the dominant pretransitional role for the lower concentrations. Unfortunately, at present, we do not have data for $\Delta\chi(T)$ at $\rho\geq 4.0$ mg/cm$^3$, so we cannot determine directly the relative degree of pretransitional behavior in $\Delta n_{\max}$ and $S$ at higher concentrations. However, we would certainly expect a significant shape effect to accompany any large change in $\Delta\chi$, and the dramatic change in $I_T$ (Fig. 5) points to a substantial structural transformation at $T_m$.

We therefore consider possibilities for a change in structure. The morphological studies, reviewed in Sec. I, demonstrate that in pure-water systems the phase for $T<T_m$ is composed of liposomes; these are also the strongest candidates [4] for isotropic aggregates in the alcohol-rich system. Moreover, as also mentioned in Sec. I, there is a strong physical basis for a tubule-liposome transition at the lipid chain-melting temperature. Below $T_m$, the highly anisotropic tubules are stabilized by orientational order in the tubule walls, while above $T_m$, the fluidity of the hydrocarbon tails favors an isotropic shape. If we assume that the isotropic structures for both the turbid and nearly transparent isotropic phases are liposomes, we may place rough limits on their size using the results for $I_T$ in Fig. 5, together with a comparison of the calculated optical depth $\tau$ (which determines $I_T$) for a solution of spherical shells with that for cylindrical shells (with $L\gg b$). This quantity is given by [27] $\tau=\nu A_g Q_{\rm sc} l$, where $A_g$ is the geometrical cross section of the particle ($2\pi R\delta$ for a spherical shell and $2L\delta$ for a cylindrical shell), $l=0.32$ cm is the sample path length, and $Q_{\rm sc}$ is the single-particle scattering efficiency defined as [27] $Q_{\rm sc}\equiv(A_gk^2)^{-1}\int d\Omega\, F(\theta,\phi)$, where $F(\theta,\phi)$ gives the distribution of the scattered intensity, $I=I_0f(\theta,\phi)/k^2r^2$. [We calculated $Q_{\rm sc}$ by extending the methods of Ref. [27] for solid particles to the case of hollow shells (i.e., two boundary surfaces). An explicit solution for spherical shells was published many years ago [28]. We do not account for scattering due to fluid membrane fluctuations,

which may contribute for large liposomes.]

For the initial tubules, and taking $\nu = 5.0 \times 10^9$ cm$^{-3}$ (about the midpoint of the experimental range), we find $\tau \approx 1.1$. For a systems of single-bilayer liposomes at the same concentration and using the same amount of lipid, we get $R \approx 2.5$ $\mu$m and $\tau \approx 4.3$. Finally, for liposomes with $\tau < 1$ and using the same amount of lipid, we find the corresponding $R < 0.15$ $\mu$m. The extinction factor $\exp(-\tau)$ of the incident light for liposomes with $R = 2.5$ $\mu$m would be about 25 times that of the tubules. This is in reasonable agreement with the observed effect in Fig. 5 at $\rho = 4.0$ mg/cm$^3$ for extinction in the turbid isotropic phase, although we have not accounted for multiple scattering, which may be expected [27] to contribute for $\tau > 3$. On the other hand, for the nearly transparent isotropic phase, our comparison of optical densities suggests particles of *maximum* size $\approx 0.1$ $\mu$m.

The details of a possible transformation at $T_m$ from tubules to comparatively small isotropic particles (when $\rho \leq 2.0$ mg/cm$^3$ and $\tau \ll 1$) are a matter for conjecture. Perhaps the loose helical fragments observed [4] to be tubule precursors in alcohol-rich systems serve as intermediaries. In fact, the presence of these structures may be experimentally reflected in the change in $\Delta\chi$ observed for $\rho = 1.0$ mg/cm$^3$ at $T$ well below $T_m$. On the other hand, for the case of very large liposomes ($\rho \geq 4.0$ mg/cm$^3$ and $\tau \gg 1$), one can construct a more specific scenario for a direct transformation between single-bilayer structures. Recent theoretical arguments [11,29] point out that a spherical vesicle cannot support a uniform molecular tilt, and that, as a result, two defects at opposite poles on the surface are inevitable. If the tilt order is sufficiently strong, these point defects would cost too much energy, and openings could spontaneously form at the defect cores. (The energetic penalty for this would be lower in an alcohol-rich system.) Moreover, if at $T_m$ the bilayer additionally develops hexatic or crystalline order, the in-layer elasticities would be anisotropic, and the bilayer surface might prefer an anisotropic topology—e.g., that of a hollow cylinder. The model of Ref. [11] does present the possibility that measurements that couple directly to shape anisotropy (e.g., $\Delta n^F_{\max}$) might reflect the development of the tilt, hexatic, or crystalline order within the bilayer.

The shape of the curves for $\Delta n_{\max}$ in Fig. 4 at $\rho \geq 4.0$ mg/cm$^3$ is suggestive of critical behavior at the tubule-(turbid) isotropic transition, and, specifically, of a crossover from a continuous transformation (in the limit where the turbid phase disappears) to a discontinuous one at higher $\rho$ (where the turbid region broadens). For $\rho = 4.0$ mg/cm$^3$, we have attempted a fit of the pretransitional data to a simple power law,

$$\Delta n_{\max} = A t^x + B \ , \quad T < T_m \ , \tag{13}$$

where $t = (T_m - T)/T_m$ and $B$ is a background term, which is needed because of the rounding of the data near $T_m$. These data points, which are not very extended ($\approx 1.8$ °C), are eliminated from the fit. Equation (13) might apply if $\Delta n_{\max}$ scales with an order parameter for the in-layer molecular order (e.g., tilt), or, perhaps as a consequence of a particle shape change, if the orientational order parameter $S$ develops a nearly continuous temperature dependence for $T \rightarrow T_m$. However, as pointed out above, we do not believe the transition is associated with purely orientational effects (e.g., a nematic-nematic critical point). Figure 6 shows the result of the fit. The fit covers the range $295\ \text{K} < T < 303.95\ \text{K}$. We determine the (fixed) value of $T_m = 303.95$ K used in the fit from our data for the sample transmission $I_T$. The results of the nonlinear least-squares fit with three free parameters are $x = 0.24 \pm 0.02$, $A = 1.3 \times 10^{-4} \pm 4.5 \times 10^{-6}$, and $B = 7.2 \times 10^{-6} \pm 9.0 \times 10^{-7}$.

This fit provides us with a compelling result, but unfortunately the rounding of our data and our consequent inability to locate $T_m$ precisely make it difficult to discuss meaningfully specific scenarios that might give rise to the simple dependence in (13). It is notable that the data for $\rho \leq 2.0$ mg/cm$^3$, where there is no turbid phase, could *not* be modeled by (13). We are currently preparing samples in the immediate vicinity of $\rho = 4.0$ mg/cm$^3$ to probe carefully the crossover in the behavior of $\Delta n_{\max}$, and to investigate more completely the possibility and nature of a critical point. Finally, although this crossover occurs for tubule concentration $\nu$ in the neighborhood of the predicted value [18] for nematic order in a hard-rod system at zero field, $\nu^* \approx 5.7(bL^2)^{-1} = 4.0 \times 10^9$ cm$^{-3}$ ($b \approx 0.4$ $\mu$m and $L \approx 60$ $\mu$m), it is not driven by the hard-rod interaction of eq. (7). This is so since the particle alignment is saturated at all $T$ ($|\mathbf{u} \times \mathbf{u}'| \approx 0$). Rather, we suggest that the crossover results from excluded-volume effects associated directly with specific shape transformations of a tubule in a dense array.

To summarize the results of Figs. 3–5, and our present discussion, we display in Fig. 7 a tentative $\rho$ versus $T$ phase diagram for fields above the saturation level for the tubule alignment. The transition temperatures along the solid line were determined from the data for $I_t$ in Fig. 5.

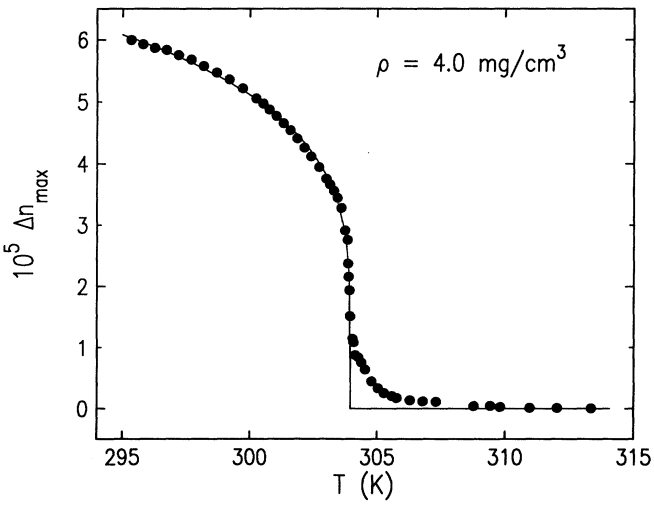


FIG. 6. Nonlinear least-squares fit of the data for $\Delta n_{\max}$ at tubule concentration $\rho = 4.0$ mg/cm$^3$. The solid line is obtained from (13).

For $\rho < 4.0$ mg/cm$^3$ (i.e., the points at 0.5, 1.0, 2.0 mg/cm$^3$), the change in $I_T$ at $T = T_m$ is not sharp. If a critical point exists along the solid line between tubule and isotropic phases in Fig. 7 for $\rho = \rho_C$ near 4.0 mg/cm$^3$, the transition for $\rho < \rho_C$ could be supercritical. At larger $\rho$, the hatched region between dashed lines suggests a coexistence between large- and small-structure isotropic phases; in this case, the regions labeled ISOTROPIC I and II are quite likely thermodynamically identical. In fact, as previously noted, the width of the hatched region depends on the heating rate, especially at $\rho = 6.0$ mg/cm$^3$, where very slow heating through $T_m$ is necessary for reproducible results.

We now turn to results for re-entrance into the tubule phase after heating to the (transparent) isotropic phase. In Fig. 8, we observe that, for low concentrations, the transition at $T_m$ exhibits a small thermal hysteresis ($< 0.1$ °C), and that the levels of $\Delta n_{\max}$ for cooling are in reasonably good agreement with those for heating. However, for the concentration $\rho = 6.0$ mg/cm$^3$ presented in Fig. 8, substantial thermal hysteresis ($\approx 0.7$ °C) is observed. The equilibrated levels of $\Delta n_{\max}$ for low temperatures also differ markedly between heating and cooling. Since our cooling data is less detailed and was obtained at a much more rapid rate, this suggests a supercooling phenomenon, which is consistent with the strongly first-order appearance of the heating data (Fig. 4) at this concentration.

The effect of the presence of the magnetic field on the phase transformation at $T_m$ and on the reformation of tubules upon cooling through $T_m$ is a subject of current investigation by us. Preliminary results are interesting and unusual. We find, for example, that the orientational order obtained after cooling the $\rho = 2.0$ mg/cm$^3$ sample in high field (Fig. 8) is extremely stable upon removal of the field [19] (this is *not* the case with the original system). Also for $\rho = 2.0$ mg/cm$^3$, a phase with anomalously large viscosity and low birefringence may be produced by cooling the sample below $T_m$ in a high field after heating in *zero* field. The viscosity and turbidity are both much higher than we have observed for aligned tubules. We have not yet determined the long-term stability of this phase. These results imply that the field is a rather important parameter in at least the short-term phase behavior of the system.

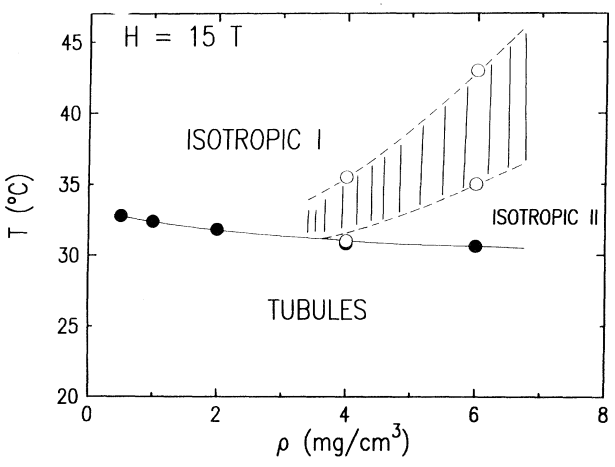


FIG. 7. $\rho$ vs $T$ phase diagram for the methanol-water system based on measurements of $I_T(T)$ and $\Delta n_{\max}(T)$ in a field for which the orientational order is saturated. If a critical point exits along the solid line in the vicinity of $\rho = 4.0$ mg/cm$^3$, the tradition at lower $\rho$ might be supercritical. Moreover, the labels I, II for the isotropic phases may primarily reflect a difference in particle size, giving rise to very different levels of sample turbidity.

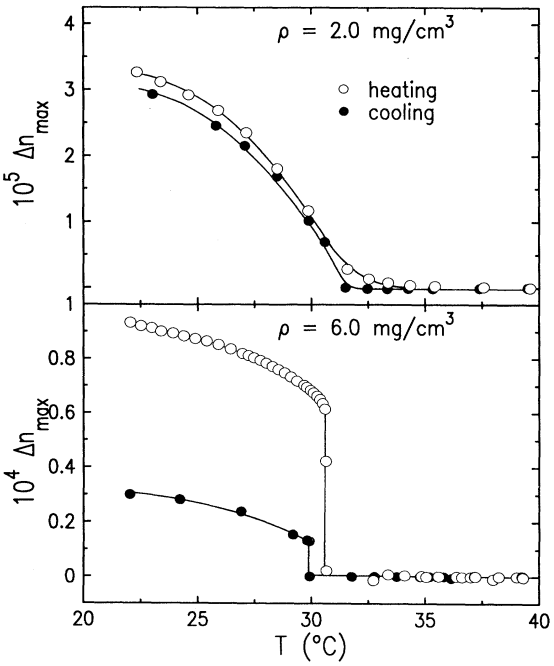


FIG. 8. $\Delta n_{\max}$ vs $T$ for heating and subsequent cooling through $T_m$ for two different tubule concentrations.

## IV. CONCLUSION

In this paper, we have described high-field magnetic-birefringence measurements on very concentrated ($\nu \approx 10^9$–$10^{10}$ cm$^{-3}$) solutions of single-bilayer and highly uniform phospholipid tubules. We find that the maximum induced refractive-index anisotropy $\Delta n_{\max}$ is a very sensitive quantitative probe of the phase transformation of aligned tubules at the lipid chain-melting temperature $T_m$, and reveals at lower $\nu$ an identical pretransitional dependence over a substantial range of $T < T_m$, and for higher $\nu$ a clear crossover to a discontinuous behavior, which coincides with the appearance of a second, very turbid isotropic phase intermediate between tubule and nearly transparent isotropic phases. For an intermediate $\nu$, corresponding to $\rho \approx 4.0$ mg/cm$^3$ for the original lipid solution, our results suggest that interesting critical behavior may be associated with the high-field tubule-isotropic transition.

The diamagnetic susceptibility anisotropy $\Delta\chi$, so far

studied only for lower concentrations, exhibits a less dramatic pretransitional behavior than $\Delta n_{\max}$, but data were difficult to obtain for $T \ll T_m$ and $T$ very close to $T_m$ (where $\Delta n_{\max} \to 0$). Comparison of these data with the results for $\Delta n_{\max}$ may also be complicated by the effect of the magnetic field on the phase diagram for the system; for the $\Delta\chi$ measurements, the temperature was changed in zero field, whereas the $\Delta n_{\max}(T)$ was studied in high field. Moreover, preliminary results of ongoing work reveal significant supercooling effects upon reforming the tubule phase after heating through $T_m$.

The present work points to a number of interesting future experiments. We are planning a magnetic-birefringence study for a narrower range of densities $\rho \sim 4.0$ mg/cm$^3$, as well as a more complete study of field-dependent effects on the phase diagram. Quasielastic light-scattering experiments are also in progress to study the structure of the high-temperature phases for the concentrations reported here; ultimately, these may be performed in high fields. Finally, more detailed data for $\Delta\chi(T)$, with the temperature changed both in zero and saturation fields, and for higher tubule concentrations, would be desirable. This quantity should be important if the molecular orientation within the tubule wall plays a significant role in the transformation to the high-temperature phase. As a final comment, we stress that the pretransitional effects for $T \to T_m$ studied in this work may be specific to single-bilayer tubules or to weakly aqueous solutions. It would be quite interesting to perform similar experiments on tubules in pure water.

## ACKNOWLEDGMENTS

The participants in this research wish to acknowledge support from several sources. Two of us (B.R. and R.S.) were supported by the Office of Naval Research, while S.S. was supported by NSF Grant No. DMR-9111389, J.D.L. was supported by NSF Grant No. DMR-9014886, and G.N. was supported by the Naval Research Laboratory through Grant No. NRL N00014-91-J-2007. We also wish to thank Sangamitra Baral-Tosh for help in preparing tubule samples, and C. Rosenblatt for a useful conversation.

## APPENDIX

In this appendix, we estimate the contributions to the maximum induced $\Delta n$ from the intrinsic molecular polarizability anisotropy and from the anisotropic tubule shape for $L \gg \lambda \gg \delta$. We consider first $\Delta n_{\max}$ from Eq. (6)

$$\Delta n_{\max} = \frac{1}{2n_0}\left[\frac{n_0^2+2n_S^2}{3n_S^2}\right]^2 \nu\Delta\alpha \ , \tag{A1}$$

where $\Delta\alpha$ is the total polarizability anisotropy per tubule. The polarizability $\alpha$ has been calculated [23] for spheroids consisting of a thin surfactant film ($\delta \ll b$) surrounding a solvent medium $A$ and immersed in a solvent medium $B$. For $A = B$, the result is

$$\alpha = O(\epsilon_s^2\beta\langle \mathbf{nn}\rangle^S + \gamma\langle 1-\mathbf{nn}\rangle^S) \ , \tag{A2}$$

where, for a cylinder (spheroid with eccentricity $=1$), the surface area $O$ of the film is $\pi bL$, $\epsilon_s$ is the solvent dielectric constant, $\mathbf{n}$ is the surface normal, $\langle\ \rangle^S$ indicates an average over the surface, and $\beta$ and $\gamma$ are the surface polarizabilities [30],

$$\beta = \delta(\epsilon_s^{-1} - \epsilon_\beta^{-1}) \ , \quad \gamma = \delta(\epsilon_\gamma - \epsilon_s) \ . \tag{A3}$$

Here $\delta$ is the film thickness, and $\epsilon_\beta$ and $\epsilon_\gamma$ are the film dielectric constants for polarizations perpendicular and parallel to the surface, respectively. Equations (A1) and (A2) are usually derived for spheroids with radial dimension less than $\lambda$; in this case, the phase of the electric field is uniform in the particle. We will shortly address the question of whether these results would apply for cylindrical shells (tubules) where the shell diameter is comparable to $\lambda$, even though the wall thickness $\delta \ll \lambda$. For the moment, we assume (A1) and (A2) to be valid.

We then obtain from (A2) and (A3), taking cylindrical coordinates with $\mathbf{n} = \mathbf{r}$,

$$\Delta\alpha = \alpha_{zz} - \alpha_{xx} = \frac{O\delta}{2}(\gamma - \epsilon_s^2\beta) = \frac{\pi bL\delta}{2}\left[\epsilon_{\perp n}^M + \frac{\epsilon_s^2}{\epsilon_{\parallel n}^M} - 2\epsilon_s\right] , \tag{A4}$$

with the dielectric constants in pure $DC_{8,9}PC$ for polarizations parallel and perpendicular to the *surface* normal $\mathbf{n}$ given by $\epsilon_{\parallel n}^M, \epsilon_{\perp n}^M$, respectively. We next let $\epsilon_{\perp n}^M = \epsilon_M - \Delta\epsilon_\perp^M(\phi)$ and $\epsilon_{\parallel n}^M = \epsilon_M + \Delta\epsilon_\parallel^M(\phi)$, where $\epsilon_M$ is the dielectric constant for an isotropic system of pure $DC_{8,9}PC$, $\phi$ is the tilt of the molecular long axis with respect to $\mathbf{n}$, and $\Delta\epsilon_\perp^M(\phi) + \Delta\epsilon_\parallel^M(\phi) = \Delta\epsilon^M(\phi) \le \Delta\epsilon_{\max}^M$, the *maximum* molecular anisotropy. Then, using these definitions, expanding (A4) for small $\Delta\epsilon^M(\phi)$, and putting $n^2 = \epsilon$ for the refractive indices, we get

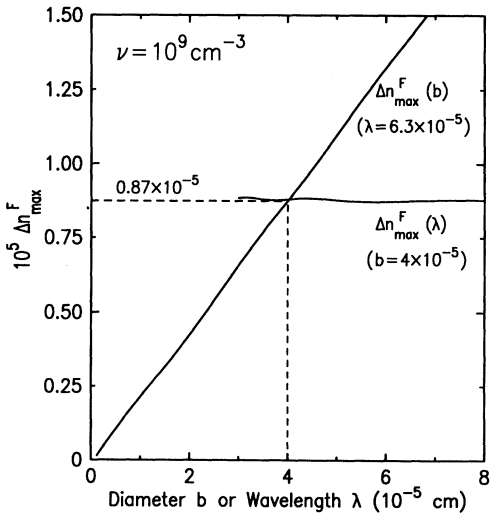


FIG. 9. $\Delta n_{\max}^F$ vs tubule diameter and wavelength calculated from scattering theory [Eq. (A7)] with $L = 60\ \mu\text{m} \gg b$, $\delta = 6$ nm, $n_s = 1.33$, $n_M = 1.50$.

$$\Delta\alpha \approx \frac{\pi b L \delta}{2}\left[\frac{(n_M^2-n_s^2)^2}{n_M^2}-\left[\Delta n_\perp^M(\phi)+\frac{n_s^4}{n_M^4}\Delta n_\parallel^M(\phi)\right]\right] . \tag{A5}$$

The first term arises from the shape anisotropy of a tubule, and the second from the intrinsic molecular anisotropy.

Taking $n_s=1.33$ (for methanol or water at 25 °C), $n_M \approx 1.50$, and for $\Delta n^M(\phi) \le \Delta n^M_{\max} \sim 0.01$ (a typical value for lyotropic materials [31]), we find that the second term is small. Since the weight fraction of lipid is very small, we take $n_0 \approx n_s$ in Eq. (A1). Then (A5) and (A1) give

$$\Delta n_{\max} \approx \Delta n^F_{\max} \approx \frac{\pi b L \delta}{4 n_s n_M^2}(n_M^2-n_s^2)^2 \nu . \tag{A6}$$

For $b=0.4$ $\mu$m, $L=60$ $\mu$m, and $\delta=6$ nm, we calculate $\Delta n_{\max} \approx \Delta n^F_{\max} \approx 0.87\times 10^{-14}\nu$. When $\nu=10^9$–$10^{10}$ cm$^{-3}$ (approximately the experimental range), this gives $\Delta n_{\max} \approx 0.87$–$8.7\times 10^{-5}$, which agrees well with the result of Fig. 4 at the lowest temperature. (For $T \to T_m$, the model of cylindrical shells without gaps probably breaks down.)

We now turn to a discussion of the assumptions made in the preceding analysis. The result (A6) has $\Delta n_{\max}$ linearly proportional to $\nu$; does this remain true even at high tubule concentrations? Indeed, one may show [32] that, for aligned *rods*, the simple proportionality is maintained for *all* $\nu$ so long as $n_M/n_s$ is close to unity. As far as the large tubule radius ($b \sim \lambda$) is concerned, we may show explicitly that the linearity of (A6) in $b$ and its independence of $\lambda$ holds so long as the shell thickness $\delta \ll \lambda$. This involves computing $\Delta n^F_{\max}$ for cylindrical shells with $L \gg b$ using Mie scattering theory [27], which is valid for any $b$ or $\delta$. (We assume an isotropic $\epsilon^M$ for convenience). We obtain, again taking $n_0 \approx n_s$,

$$\Delta n^F_{\max} = \frac{2\nu L}{n_s k^2}\sum_{n=-\infty}^{\infty}\left\{\frac{[m^2A_1(n)+mA_2(n)+A_3(n)][m^2B_1(n)+mB_2(n)+B_3(n)]}{[m^2A_1(n)+mA_2(n)+A_3(n)]^2+[m^2B_1(n)+mB_2(n)+B_3(n)]^2} - \frac{[A_1(n)+mA_2(n)+m^2A_3(n)][B_1(n)+mB_2(n)+m^2B_3(n)]}{[A_1(n)+mA_2(n)+m^2A_3(n)]^2+[B_1(n)+mB_2(n)+m^2B_3(n)]^2}\right\}, \tag{A7}$$

where $m \equiv n_M/n_s$, $k=2\pi/\lambda$, and the quantities $\{A(n)\}$ and $\{B(n)\}$ are given by

$$A_1(n)=J_n(x_0)J_n(x_1)[J_n'(y_1)Y_n'(y_0)-J_n'(y_0)Y_n'(y_1)] ,$$

$$A_2(n)=J_n'(x_0)J_n(x_1)[J_n(y_0)Y_n'(y_1)-J_n'(y_1)Y_n(y_0)] + J_n(x_0)J_n'(x_1)[J_n'(y_0)Y_n(y_1)-J_n(y_1)Y_n'(y_0)] ,$$

$$A_3(n)=J_n'(x_0)J_n'(x_1)[J_n(y_1)Y_n(y_0)-J_n(y_0)Y_n(y_1)] ,$$

$$B_1(n)=J_n(x_0)Y_n(x_1)[J_n'(y_1)Y_n'(y_0)-J_n'(y_0)Y_n'(y_1)] .$$

$$B_2(n)=J_n'(x_0)Y_n(x_1)[J_n(y_0)Y_n'(y_1)-J_n'(y_1)Y_n(y_0)] + J_n(x_0)Y_n'(x_1)[J_n'(y_0)Y_n(y_1)-J_n(y_1)Y_n'(y_0)] ,$$

$$B_3(n)=J_n'(x_0)Y_n'(x_1)[J_n(y_1)Y_n(y_0)-J_n(y_0)Y_n(y_1)] .$$

Here $J_n$ and $Y_n$ are ordinary Bessel function of the first kind; primes indicate derivatives. The arguments are $x_0=kn_s(b/2-\delta)$, $x_1=kn_sb/2$, $y_0=kn_M(b/2-\delta)$, and $y_1=kn_Mb/2$. The result (A7) is plotted in Fig. 9 versus the radius $b$. $n_s$, $n_M$, $\delta$, and $L$ were fixed to the values taken above. We see that $\Delta n_{\max}$ is linear in $b$ in the range of interest and that it is essentially independent of $\lambda$ for optical $\lambda$. Moreover, its magnitude for $b=0.4$ $\mu$m and $\nu=10^9$ cm$^{-3}$ is identical to the result obtained from (A6).


*Also at Dept. of Biochemistry, Georgetown University Medical Center, Washington, D.C. 20007.

[1] P. Yager and P. E. Schoen, Mol. Cryst. Liq. Cryst. **106**, 371 (1984); P. Yager, P. E. Schoen, C. Davies, R. Price, and A. Singh, Biophys. J. **48**, 899 (1985).

[2] N. Nakashima, S. Asakuma, and T. Kunitake, J. Am. Chem. Soc. **107**, 509 (1985); J.-H. Fuhrhop, P. Schneider, E. Boekema, and W. Helfrich, *ibid.* **110**, 2861 (1988).

[3] A good review is J. M. Schnur, R. Price. P. Schoen, P. Yager, J. M. Calvert, J. Georger, and A. Singh, Thin Solid Films **152**, 181 (1987).

[4] J. H. Georger, A. Singh, R. Price, J. M. Schnur, P. Yager, and P. E. Schoen, J. Am. Chem. Soc. **109**, 6169 (1987).

[5] B. R. Ratna, S. Baral-Tosh, B. Kahn, J. M. Schnur, and A. S. Rudolph (unpublished).

[6] P. Yager, R. R. Price, J. M. Schnur, P. E. Schoen, A. Singh, and D. G. Rhodes, Chem. Phys. Lipids **46**, 171 (1988).

[7] P. G. de Gennes, C. R. Acad. Sci. **304**, 259 (1987).

[8] W. Helfrich and J. Prost, Phys. Rev. A **38**, 3065 (1988).

[9] B. R. Ratna (private communication).

[10] W. Helfrich, J. Chem. Phys. **85**, 1065 (1986).

[11] T. C. Lubensky and Jacques Prost. J. Phys. II (Paris) **2**, 371 (1992).

[12] D. G. Rhodes, S. L. Blechner, P. Yager, and P. E. Schoen, Biochim. Biophys. Acta **902**, 349 (1988).

[13] M. Caffrey, J. Hogan, and A. S. Rudolph, Biochemistry **30**, 2134 (1991).

[14] C. Rosenblatt, P. Yager, and P. E. Schoen, Biophys. J. **52**, 295 (1987).

[15] Z. Li, C. Rosenblatt, P. Yager, and P. E. Schoen, Biophys. J. **54**, 289 (1988); D. M. Woods, Z. Li, C. Rosenblatt, P.

Yager, and P. E. Schoen, Mol. Cryst. Liq. Cryst. **167**, 1 (1989); M.-H. Lu and C. Rosenblatt, Appl. Phys. Lett. **56**, 590 (1990).
[16] L. Onsager, Ann. N.Y. Acad. Sci. **51**, 627 (1949).
[17] M.-H. Lu and C. Rosenblatt, Mol. Cryst. Liq. Cryst. **210**, 169 (1992).
[18] M. Doi and S. F. Edwards, *The Theory of Polymer Dynamics* (Oxford University Press, London, 1986), Chap. 9 and 10.
[19] S. Sprunt, G. Nounesis, J. D. Litster, B. Ratna, and R. Shashidhar, Phys. Rev. E **47**, 3477 (1993).
[20] See, for example, G. Maret and K. Dransfeld, *Biomolecules and Polymers in High Steady Magnetic Fields,* edited by F. Herlach, *Topics in Applied Physics* Vol. 57, (Springer-Verlag, New York, 1985).
[21] B. D. Larson, Ph.D. thesis, Massachusetts Institute of Technology, 1986 (unpublished); S. N. Jasperson and S. E. Schnatterly, Rev. Sci. Instrum. **40**, 761 (1969).
[22] M. R. Battaglia and G. L. D. Ritchie, J. Chem. Soc. Faraday Trans. 2 **73**, 209 (1977).
[23] E. van der Linden, S. Geiger, and D. Bedeaux, Physica A **156**, 130 (1989).
[24] A. D. Buckingham and J. A. Pople, Proc. Phys. Soc. **69**, 1133 (1956); A. Peterlin and H. A. Stuart, Z. Phys. **112**, 1 (1939).
[25] W. Maier and A. Saupe, Z. Naturforsch. **13A**, 564 (1958); **14A**, 882 (1959); **15A**, 287 (1960).
[26] P. G. de Gennes, *The Physics of Liquid Crystals* (Clarendon, Oxford, 1974), Chap. 2.
[27] H. C. van de Hulst, *Light Scattering by Small Particles* (Dover, New York, 1981).
[28] A. L. Aden and M. Kerker, J. Appl. Phys. **22**, 1242 (1951).
[29] Ou-Yang Zhong-can and Liu Ji-xing, Phys. Rev. A **43**, 6826 (1991).
[30] D. Bedeaux and J. Vlieger, Physica **67**, 55 (1973).
[31] See, for instance, B. D. Larson and J. D. Litster, Mol. Cryst. Liq. Cryst. **113**, 13 (1984).
[32] W.L. Bragg and A. B. Pippard, Acta Crystallogr. **6**, 865 (1953).